Australian Journal of Basic and Applied Sciences, 6(9): 693-701, 2012
ISSN 1991-8178

Application of Spectral Induced Polarization (SIP) Imaging for Characterizing the Near-Surface Geology: An Environmental Case Study at Schillerslage, Germany

[1,2]Mohamed Attwa and [3]Thomas Günther

[1,2]Geology Department, Faculty of Science, Zagazig University, 44519 Zagazig, Egypt.
[2]Present address: Geophysical Engineering Department, Faculty of Engineering, Ankara University, 6200 Ankara, Turkey.
[3]Leibniz Institute for Applied Geophysics (LIAG), 30655 Hannover, Germany.

Abstract: Spectral **i**nduced polarization (SIP) imaging is a promising tool for environmental studies. Application of this method for the near-surface investigations has previously been limited by incomplete understanding of the physicochemical controls on the IP response, with a lack of appropriate methods for data inversion. We aim to study the applicability of the 2D IP imaging for resolving the near-surface sediment heterogeneity, as well as the Quaternary aquifer at Schillerslage test-site in the north of Germany. An SIP survey was carried out along four profiles with dipole-dipole configuration using different electrode spacings. Multi-frequency data were recorded and inverted with a 2D smoothness constrained inversion to obtain the 2D images of conductivity magnitude, phase, real and imaginary parts of conductivity for each frequency. Displaying all these parameters is redundant, but reflects different subsurface characteristics. The 2D inversion results were correlated with the borehole information. The inverted 2D sections discriminate the soil, peat, saturated sand and the till layer. The peat and sandy aquifer can be recognized well from the phase images, while the till layers can be discriminated from the conductivity imaginary images. On the other hand, the conductivity magnitude and the real part of conductivity images show monotonous changes of conductivity with depth. However, the range of IP response observed in these sediments complicates the lithologic interpretation. Moreover, further laboratory work is needed to better understand the effects of micro-geometry, as well as the physical and chemical processes controlling the observed IP.

Key words: Spectral induced polarization (SIP); IP imaging; Near-surface geology.

INTRODUCTION

Geophysical exploration techniques have been increasingly used to infer the properties of the saturated and unsaturated zones. Besides the advantages of minimal disturbance to the subsurface, geophysical methods have a significant advantageous over the conventional hydrogeological measurements. They provide measurements over relatively large supported volume. Electromagnetic induction, direct current resistivity and ground penetrating radar have been widely used in the hydrogeological studies to infer lithologic boundaries and to help in the development of conceptual models of the subsurface geology.

The induced polarization (IP) method is an extension to the well-known geoelectric technique. The effect of IP was discovered at the beginning of the 20th century by Schlumberger brothers. However, it was not popular till the middle of the last century. The high polarization effect of the conductive minerals made it possible to use IP measurements for ore-exploration. On the other hand, non-metallic rocks show a polarization effect, relatively small, but still measurable with improving technology. So the IP measurements became more established in the last twenty years (Klitzsch, 2004).

The method of spectral induced polarization (SIP) measures the frequency-dependent complex electrical rock conductivity. Real and imaginary parts of the electrical conductivity are influenced in different ways by parameters describing pore space structure and fluid properties. SIP measurements yield both amplitude and phase spectra of electrical conductivity. Recent advances in the IP instrumentation and modeling algorithms, combined with a better understanding of the physical significance of IP response, encourage field-scale applications of the method (Kemna *et al*., 2012).

Environmental and engineering applications of the IP method have emerged from laboratory studies of measurable IP effects associated with non-metallic minerals (e.g. Börner *et al*., 1996). It is known that, the interface between a non-metallic mineral and a saturating fluid is polarized, as a result of redistribution of ions along the interface, following the propagation of electrical current. Upon current termination, ions relax back to the equilibrium, the resulting residual current flow being the source of the subsurface IP response. A strong IP effect is observed in sediments containing clays disseminated on the surface of larger grains. Hence, shaly sand/silty and shaly sandstone typically displays large IP effects (e.g., Klein and Sill; 1982; Sturrock *et al*. 1998;

Corresponding Author: Mohamed Attwa, Geophysical Engineering Department, Faculty of Engineering, Ankara University, 6200, Ankara, Turkey.
E-mail: attwa_m2@yahoo.com

Attwa *et al*., 2009; Attwa *et al*., 2011; Attwa, 2012). In contrast, compacted clays are usually associated with low IP effects, as the ohmic conduction dominates current flow. Small measurable IP effects are associated with clean sand and gravel (Vanhala, 1997).

In the present work, surface multi-channel SIP measurements were carried out to study the aquifer characterization of the sand/gravel aquifer at the hydrogeological test-site of Schillerslage, Germany. The role of SIP in discovering the lithologic heterogeneity was emphasized, as these are a fundamental to hydraulic conductivity estimation. Further, the IP response of peat layer intercalated within the sandy aquifer at this test-site, was described. Although the measurements were carried out over a broad frequency range (i.e. SIP), our interpretation was restricted to single low frequency data, to avoid the induction effects at high frequencies.

Local Geology:

The Schillerslage test-site (52^{o} 29` 45`` N, 9$^{o}$ 58` 10`` E) is located 20 km northeast of Hannover in the north German plain (Fig.1). The test-site was chosen by Leibniz Institute for Applied Geophysics (LIAG) to assess the different novel geophysical methods. The actual test-site includes 3.5 ha, partly forested, but mostly grassland. Several boreholes were drilled to get cores and soil samples.

The area is characterized by para- and preglacial unconsolidated sediments (Jordan, 1975). The new test site of Schillerslage shows a typical geological structure for the North-Germany Quaternary sediment basin: two sandy aquifers, separated by a fine-grained till layer, are overlying Cretaceous marl (Fig.1). The upper aquifer, down to a depth of 12 to 13 m, consists of medium to partly coarse sands with interbedded thin peat layers. The aquiclude till layer with high clay content is of about 12 to 16 m deep and varies also in thickness. The lower aquifer of 5 m thickness consists of slightly limy medium grey sand and it is overlying the Cretaceous marl.

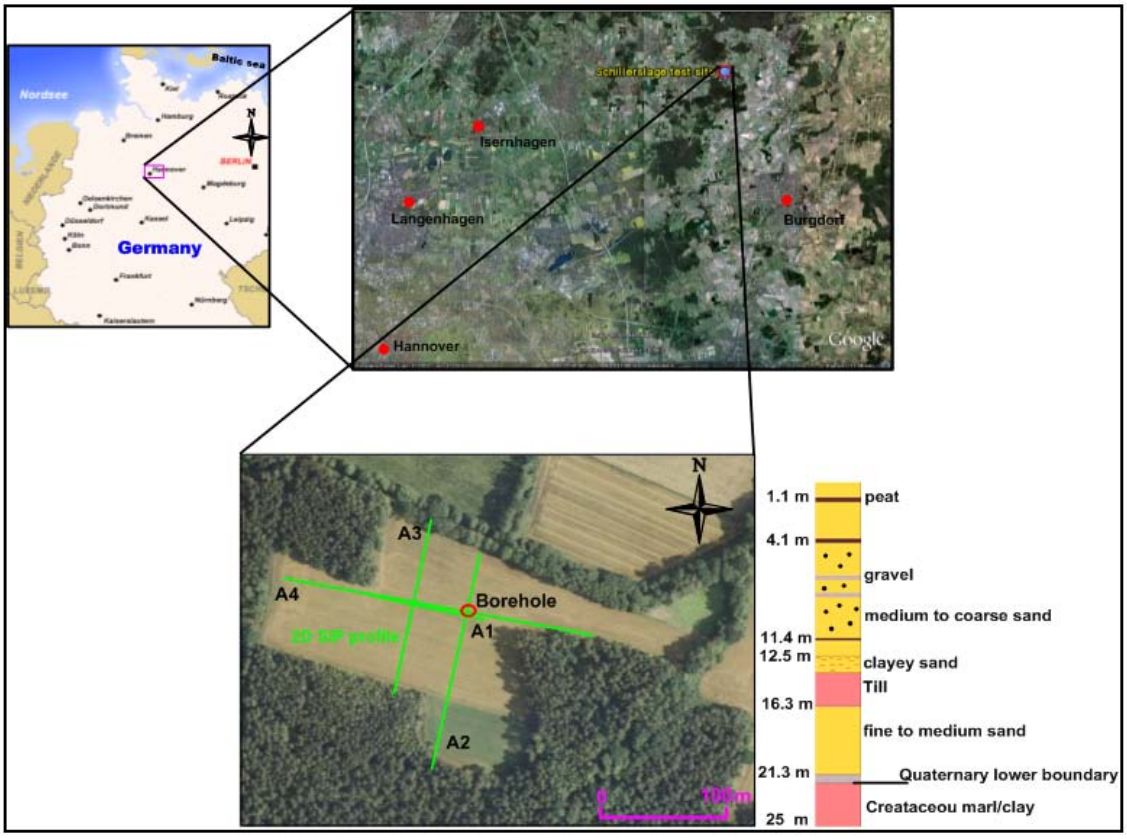

Fig. 1: (top) Schillerslage test-site (Hannover) and (bottom) location of the measurements and local geology according a borehole. A1-A4 are 2D SIP profile numbers.

Method and Survey:

Spectral induced polarization (SIP), also called complex resistivity (Lange and Jacobs, 2005), is an impedance-spectroscopy method to determine the polarization characteristics of soils and rocks. The principles of the method are based on the change of electro-chemical and electronic conductivity caused by variations of mobility of the ions in the electrolyte in the pore spaces of the rocks and therefore also in soil (Seidel and Lange, 2005).

In the SIP method, the electric resistivity and phase angle are measured over a wide range of frequencies (typically from 0.625 Hz to 10 kHz). Several authors described the correlation between the frequency spectra and the petrophysical parameters; such as grain size, pore size and tortuosity (e.g. Hördt *et al*., 2009). Recent reviews of the method, including a brief discussion of the underlying mechanisms are given by Slater and Lesmes (2002), Kemna *et al*. (2004), Revil and Florsch, 2010 and Weller *et al*., 2010, and references therein. In the SIP method, the fundamental quantities of interest are the electrical conductivity magnitude $|\sigma(\omega)|$ and phase $\varphi(\omega)$ (or the equivalent real and imaginary parts of conductivity) of complex conductivity as a function of frequency as:

$$|\sigma(\omega)| = ((\sigma')^2+(\sigma'')^2)^{0.5} \quad (1)$$

$$\sigma' = |\sigma(\omega)|\cos\varphi \ \ and \ \ \sigma'' = |\sigma(\omega)|\sin\varphi \quad (2)$$

where: ω is the angular frequency and σ' and σ'' are the real and imaginary parts of the electrical conductivity, respectively.

Spectral induced polarization measurements were carried out along four 2D profiles (Fig.1, bottom). Three of the profiles (A1, A2 and A4) are crossing the location of the drilled borehole. These data were recorded with a broad frequency range, from 0.625 Hz to 10 kHz. The 2D profiles were measured using 36 electrodes with different electrode spacings to obtain different subsurface geological information, and to characterize the heterogeneity and subsurface sandy aquifers. To minimize the induction effects (Hördt *et al*., 2007), the dipole-dipole configuration was used to acquire the 2D IP data. The A1 profile was measured using 2 m electrode spacing. Electrode spacings of 4 m, 5 m and 7 m were used to acquire the 2D data across the A3, A2 and A4 profiles, respectively (Fig.1, bottom). Profiles A1 and A3 are crossing at a borehole with known lithology, to control the inversion procedures of the IP data.

Data Recording and 2D Inversion:

In the present survey, the multichannel equipment SIP256C (Fig. 2) by Radic Research (Radic *et al*., 1998 and Radic, 2004) was used to collect the data along the four profiles. In this system, each steel electrode is connected to a remote unit, which registered the voltage and current measurements, digitized the data and transferred them to a controlling PC through a fiber optics cable, to avoid the interference of the current supply cables with the voltage dipoles. Acquisition of the very low frequency data is limited by the data acquisition time. For one profile, it is several hours (more than 2 hours) and can easily become excessive, if even lower frequencies (< 0.625 Hz) are required, even though the system efficiently measures the voltages at all receiver channels simultaneously.

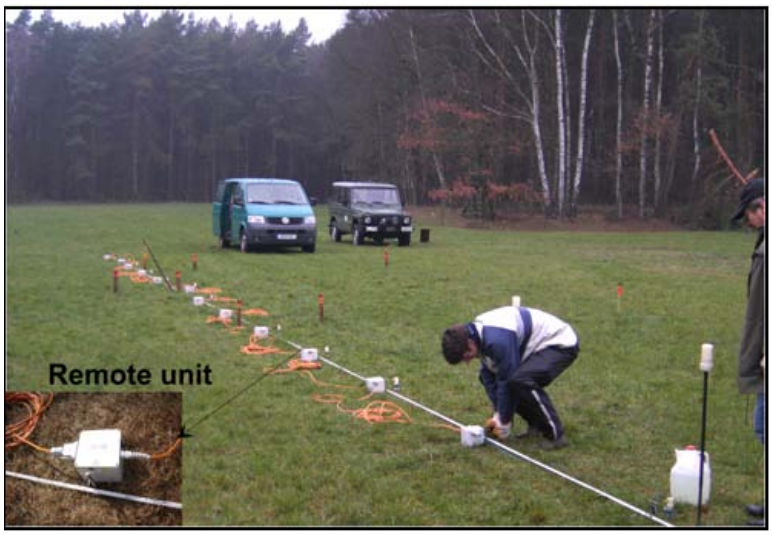

Fig. 2: The multichannel SIP equipment by Radic Research (Radic 2004) in operation at a Schillerslage test site in North Germany.

For the SIP data, inspection of the complex resistivity data is required to select the best frequencies for the 2D inversion process. To detect the EM coupling effect, the measured SIP data were plotted vs. frequencies for different dipole lengths. Figure 3 shows a sample of a SIP measured data set that, displayed as φ_a (bottom) vs. frequencies, using 2 m dipole length with different dipole distances. The φ_a values are almost constant over a

limited range of frequencies up to 10 Hz and show capacitive coupling at higher frequencies (> 10 Hz). The capacitance is created by wires, chassis, and other, metal components of electronic equipment and field wires. Attempts have been made to remove the capacitive coupling from the data (e.g., Xiang *et al*., 2002 and Radic, 2004), but here we used data in the range below 10 Hz, where the data were not significantly affected.

Data processing and inversion were carried out using DC2DInvRes software (Günther, 2004). This software uses finite difference forward modeling to calculate the apparent resistivity values and the non-linear least-square optimization technique is used for inversion routine (deGroot-Hedlin and Constable, 1990 and Loke and Barker, 1996). A Gauss-Newton algorithm, using smoothness constraint with fixed regularization, was chosen for the 2D inversion. The 2D inversion algorithm was implemented for a global regularization scheme, using a first-order smoothness constraint (Günther, 2004). As introduced by Constable *et al*. (1987), different weights were used for horizontal and vertical model boundaries; such that: $a_x = \lambda$ and $a_z = \lambda w_z$. The regularization parameter (λ) is a weight for the model smoothness constrains against the data misfit. A small value of λ (or w_z) will produce a highly structured model with huge parameter contrasts, explaining the data well, whereas a big value will not be able to fit the data, but provides a smooth model.

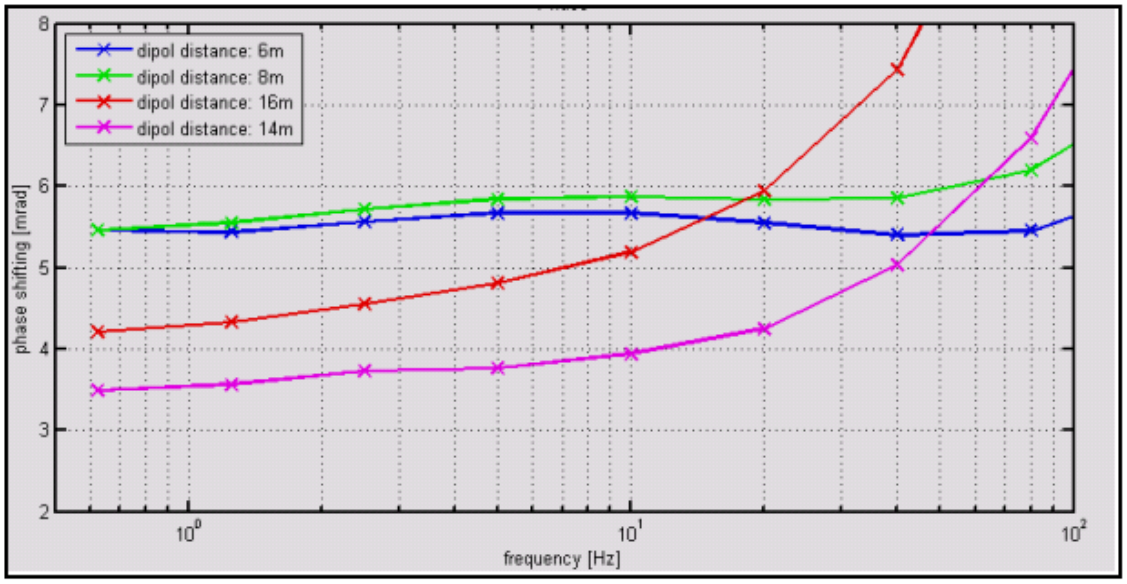

Fig. 3: Phase vs. frequency of dipole-dipole array, 2 m in length with different dipole distances.

To avoid the distortion by the coupling effect, only low frequency data were used in the inversion process. The 2D processing included the rejection of bad quality data points from the measured data, i.e. for which the stacking error was above 1%. In addition, in absence of reciprocal data, 3% error was added to the stacking error to account for systematic error components. In the IP inversion process, first the DC potentials are inverted to recover a background resistivity magnitude and then the distribution of phase can be found by linearizing the IP data equation and solving a linear inverse problem (Beard *et al*., 1996 and Kemna, 2000). After each iteration, an improved resistivity estimate is sought and eventually the procedure stops until certain convergence criteria are met.

Figure 4 shows an example of a processed complex resistivity data set (1091points) along profile A1 (Fig. 1) at 0.625 Hz in the form of apparent resistivity sections (left) and histograms (right); note that the A1 profile length is related to the A4 profile (see Fig.1). In this data set, it was observed that, for larger dipole distances, the measured phase values were higher than the surrounding points, which can be attributed to the EM coupling. It is clear that, the pseudo-sections do not exhibit a clear layering, but show variations in the $|\rho_a|$ and φ_a values. In general, the inversion process is able to simulate the measured data. In addition, because of using an asymmetrical dipole-dipole configuration, i.e., unequal dipole length, the values of dipole length a cannot be written on the z-axis of either $|\rho_a|$ and φ_a pseudo sections (Fig. 4, top and bottom, respectively).

Results:

Figure 5 shows the results of the electrical resistivity tomography (ERT) survey of the profile A1 (Fig. 1, bottom). The inspection of SIP inverted data in comparison with the borehole information indicates that IP response can be presented using the low frequency (e.g., 0.625 Hz) IP data to avoid the EM coupling effect. The inversion results of 0.625 Hz were enlarged and presented in the form of conductivity magnitude |σ|, the conductivity real part σ', the phase φ and the conductivity imaginary part σ'' . Both the phase and magnitude

parameters are independent. On the other hand, both the real and imaginary parameters are equal to the multiplication of the independent parameters $|\sigma|$ and φ. The images coincide well with the available borehole data. For the 2D inversion, the regularization anisotropy was set to $w_z = a_z/a_x = 0.01$, in order to achieve predominantly layered structures. A good agreement can be observed between the borehole data and the phase inversion results.

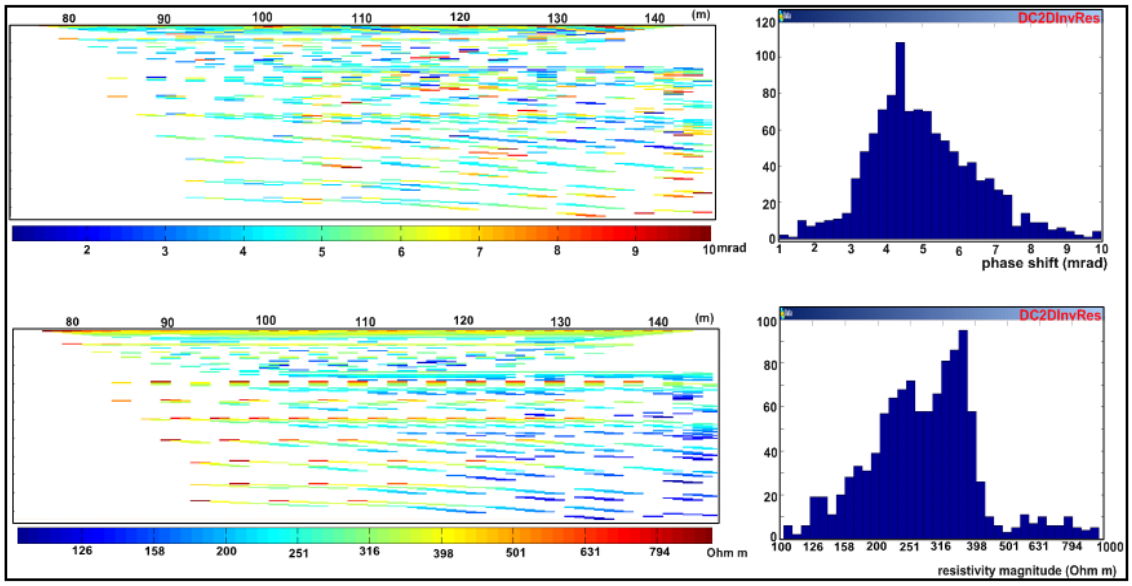

Fig. 4: Top: (left) phase pseudosection and (right) histogram at 0.625 Hz. Bottom: (left) measured apparent resistivity section and (right) histogram at 0.625 Hz.

In general, $|\sigma|$ and $\sigma`$ are directly proportional to the electrolytic conduction in connected pore spaces by ionic migration. Therefore, the conductivity magnitude images (Fig. 5a) and the real conductivity images (Fig. 5b) show the same features of an upper low conductive layer (< 0.0063 S/m), with 11 m maximum thickness, corresponding to the upper sandy aquifer. The discrimination between the heterogeneities of thin layers within the upper sandy aquifer cannot be achieved from the $|\sigma|$ and $\sigma`$ images. The sandy aquifer overlies a high conductivity layer (~0.015 S/m), that corresponds to till layer.

The phase images (Fig. 5c) show additional geologic information within the unconsolidated deposits. The phase image shows an upper layer of low phase values, corresponding to the near surface sandy layer. This layer overlies a moderate phases (~ 9 mrad), which corresponds to the peat layer. At ~ 1.87 m depth, a third low phase layer can be observed, which corresponds to the upper sandy aquifer. At about 13 m depth, there is a sharp boundary between low (< 4 mrad) and high phase values (> 13 mrad), which corresponds to the boundary between the lower sandy aquifer and the till layer. The upper sandy aquifer, of low phase values, coincidences with the borehole data.

The discrimination between the fine sediments and/or clay and the sandy layer can be even better imaged and characterized by the imaginary part (Fig. 5d), which is a combination of the magnitude and phase data, but it is dominated by the conductivity magnitude values. A shallow medium conductivity layer can be observed at ~1.2 m (Fig. 5d), corresponding to the peat occurrence. The images of imaginary part show a highly conductive layer at ~12 m. It corresponds to the till layer and clay. It is clear that the imaginary conductivity image introduces new information about the lithologic heterogeneity within the Quaternary unconsolidated sediments compared to the real conductivity image.

The study of both the sensitivity analysis and the inversion results of IP data are redundant to evaluate the accuracy of the interpretation. According to Günther (2004), the zones of higher coverage values indicate that, the reliable parts of the model as derived from the inverted data. Consequently, the maximum depth of sensitive area is about 17 m (Fig. 5e) and beyond this depth, the data will lose the capability to resolve the heterogeneity between sedimentary layers. Accordingly, the heterogeneity within the upper aquifer can be well recognized (Fig. 5e).

The inversion results of the other 2D profiles (A2 to A4) showed no great differences to A1, except for penetration depth. To avoid the repetition of the 2D models interpretation, the models are shown in the form of 3D fence diagrams (Figs. 6). Similar to the A1 profile, we choose the 0.625 Hz data for presentation and further discussion, using the same regularization parameter of the z-weight (w_z).

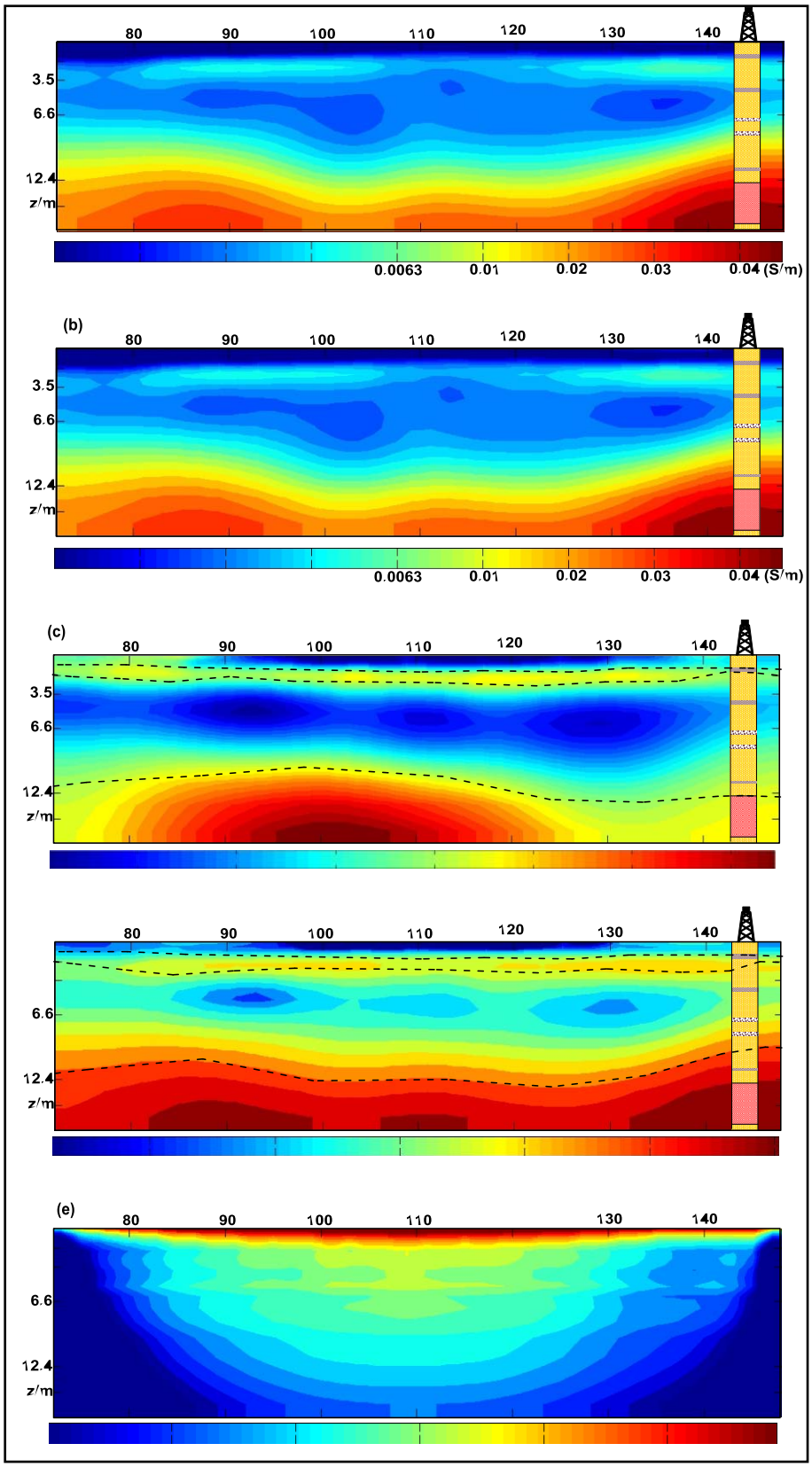

Fig. 5: Conductivity magnitude (a), real part of conductivity (b), phase shift (c), imaginary part of conductivity (d) and coverage section (e) of profile A1 in the 2D image plane as determined by complex resistivity inversion at 0.625 Hz. The A1 profile length is related to the A4 profile (see Fig.1).

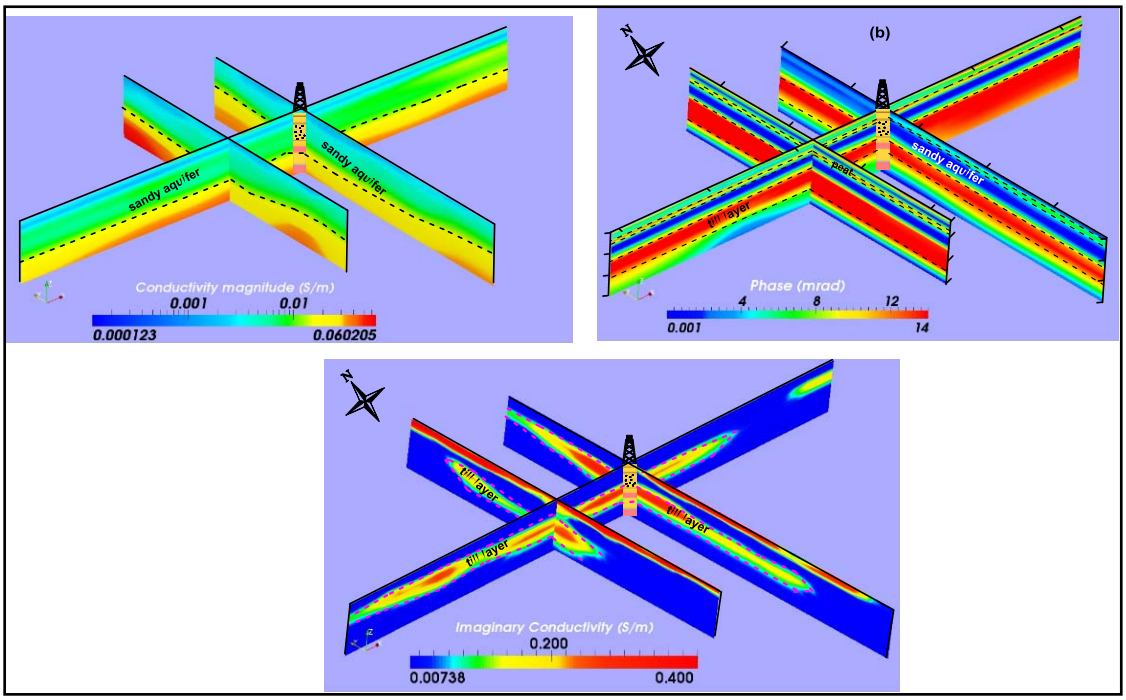

Fig. 6: 3D fence diagram of ERT in the form of Conductivity magnitude (a), phase shift (b) and imaginary part of conductivity (c) at 0.625 Hz. A2, A3 and A4 are the 2D profile numbers, for location see Fig. 1.

Figure 6 reflects that, displaying all the three parameters, i.e. conductivity magnitude, phase and imaginary part of the conductivity, is redundant. The fence diagram indicates that, below the resistive soil, the conductivity magnitude (Fig. 6a) monotonically increases with depth. The conductivity phase (Fig. 6b) behaves differently, showing a thin layer with high values roughly at 4 m depth, embedded between a zone of medium phase shift, which overlies a very low phase shift layer, corresponding to the upper sandy aquifer. At about 12 m depth, a very high phase shift layer can be observed, which corresponds to the till layer. Its thickness is about 7 m, except for the eastern part of the area (i.e. A4, see Fig. 1), where it cannot detect its thickness. This can be attributed to the low data coverage at the eastern part of profile A4, which was caused by using the asymmetrical dipole-dipole array and rejecting the bad quality data points. This layer overlies a medium to low phase shift layer.

Discussion:

The previous work has shown the phase and imaginary conductivity images may reflect different subsurface characteristics and thus looking at both of them can be instructive (Kemna *et al*., 2004). Figure 6c shows an agreement with the available borehole lithologic information (Fig.1), which can be attributed to the increase of σ'' with the pore-surface-related internal surface. However, due to the smoothness constraint, the different layers are not well defined and cannot easily be related to the known lithology. The high values of the imaginary conductivity (Fig. 6c) can be attributed to the till layer. The disappearance of this layer at 23.6 m depth can be caused by the low data coverage. The near surface alyer of high imaginary part of conductivity values, corresponding to the peat layer, can be observed along A2 and A3 only. The absence of this layer along A4 profile can be related to the use of 7 m electrode spacing during the data acquisition.

The overall images (Fig. 6) reflect the anticipated geology: well defined zones, as well as predominately horizontal and smooth lateral variations within the zones. The images look realistic and coincid well with the known lithology given in Fig. 1. The near-surface thin peat layer between 1 m and 4 m appears as a distinct layer with low conductivity magnitude and high phase shift. The imaginary conductivity images of both A2 and A3 profiles (Fig. 6c) show good distinction of the near-surface peat layers. On the other hand, there is a little discrimination of the near-surface peat layer in the σ'' image along A4 profile indicating that, the electrical property variations within the near-surface layer are below the resolution limit. This can be attributed to the increase of the electrode spacing during the data acquisition of A4, which decreases the resolution of the 2D model and, consequently, the conductivity magnitude is dominated over phase shift parameter. The top of the upper sandy aquifer appears in the phase image as sharp boundary, whereas it is less prominent in the conductivity magnitudes. A sharp contact between the upper sand aquifer and the till layer can be well defined from both phase and imaginary conductivity images (Fig. 6 b and c). It is noticed that, the lower sandy aquifer cannot be differentiated from the upper till layer. This can be attributed to the presence of a high phase layer (till) above the lower aquifer, which decreases the resolution with increasing depth, and/or the low data coverage

with increasing the depth. Similarly, at about 23.6 m depth, the Cretaceous marl layer of low phase values (< 7 mrad) cannot be recognized at the eastern part of the profile A4.

In Figs. 5 and 6, the inverted model parameters illustrate how the phase shift and imaginary part of conductivity discriminate between the polarization and bulk conduction effects. Based on the inversion results of the 2D profiles, it is clear that, the upper aquifer can be well defined, but we still have limitations in imaging the lower one. These limitations include an electromagnetic coupling with increasing the current electrode spacing and the penetration depth of the 2D imaging. In general, our field inversion results indicate that, the upper and lower boundaries of the upper aquifer (1^{st}) can be well defined from the phase values. The upper boundary of the lower sandy aquifer (2^{nd}) is deeper than in reality, which can be attributed to the electrical behavior at resistivity boundaries; more current will travel through conductive (till) layer in preference to resistive (sands) layers. The results is that the current density at the upper boundary of the lower sandy aquifer is decreased, and so the potential gradient will decrease across the boundary (Kilner *et al*., 2005).

The value of the IP measurement is that, it helps to distinguish the saturated sandy aquifers from the clay-rich zones (e.g., till and peat), which exhibit low resistivity, but relatively high chargeability. Zanetti *et al*. (2011) reported high phase values for the buried tree root samples using laboratory experiments. They showed that a regular distribution of the pore size in diffuse porous woods leads to a stronger polarization effect. Because the peat layer also contains plant remains, the 2D IP profiles show a high polarization effect.

Conclusions:

The presented field study results illustrate the general value of IP imaging for improved subsurface characterization, as it provides unique information on the strength of low-frequency polarization occurring in the subsurface. Our study highlights the potential value of IP imaging for differentiating lithological units and characterizing the heterogeneity of these units. The subsurface of the area under consideration is characterized by strong variations in the subsurface conditions as a result of the heterogeneity of its constitutes and can change over short distances. The phase and imaginary conductivity images (SIP measurements) reflect independent subsurface characteristics. Whereas the real conductivity is a function of both electrolytic and surface conductivity terms, the imaginary conductivity is predominantly a measure of surface conductivity, and thus well correlated with fine sediments of peat and till layers. Similarly, the conductivity phase reveals an accurate detection of the peat and till layers compared to the real resistivity image. However, it is clear that the IP imaging has a limited applicability especially in existence of highly heterogeneity because the resolution decreases with increasing depth. Smooth model inversion with adapted regularization parameters improves the interpretability of IP data. Consequently, the use of IP imaging favors for investigating lithologic variability in near-surface, unconsolidated sediments.

Further fundamental investigations of the dependence of IP effect on the key lithologic parameters are required. In addition to further work, including SIP lab measurements, is recommended to study the spectral behavior of the till layer.

ACKNOWLEDGMENT

Our investigations were a part of the hydrogeophysical research project at Schillerslage test site, Leibniz Institute for Applied Geophysics (LIAG), Hannover, Germany. I wish to extend warm thanks to Raphael Holland for his help and assistance during the field work. I also thank the Scientific Research Council of Turkey (TÜBITAK) for assistance in publishing this manuscript.

REFERENCES

Attwa, M., 2012. Electrical methods: A practical guide for resistivity imaging and hydrogeophysics. LAP LAMBERT Academic Publishing GmbH and Co. KG, 218 pp.

Attwa, M., T. Günther, M. Grinat and F. Binot, 2009. Transimissivity estimation from sounding data of Holocene tidal flat deposits in the North Eastern part of Cuxhaven, Germany. Extended Abstracts, Near Surface Geophysics - 15th European Meeting of Environmental and Engineering Geophysics, 29.

Attwa, M., T. Günther, M. Grinat and F. Binot, 2011. Evaluation of DC, FDEM and SIP resistivity methods for imaging a perched saltwater and shallow channel within coastal tidal sediments, Germany. Journal of Applied Geophysics, 75: 656-670.

Beard, L.B., G.W. Hohmann and A.C. Tripp, 1996. Fast resistivity/IP inversion using a low contrast approximation. Geophysics, 61: 169-179.

Börner, F.D., W. Schopper and A. Weller, 1996. Evaluation of transport and storage properties in the soils and groundwater zone from induced polarization measurements. Geophysical Prospecting, 44: 583-601, doi:10.1111/j.1365-2478.1996.tb00167.x.

Constable, S.C., R.L. Parker and C.G. Constable, 1987. Occam's inversion: A practical algorithm for generating smooth models from EM sounding data. Geophysics, 52: 289-300.

Günther, T., 2004. Inversion methods and resolution analysis for the 2D/3D reconstruction of resistivity structures from DC measurements. Ph.D. thesis, Technische Univ., Freiberg, Germany.

deGroot-Hedlin, C. and S. Constable, 1990. Occam's inversion to generate smooth, two dimensional models form magnetotelluric data. Geophysics, 55: 1613-1624.

Hördt, A., R. Blaschek, A. Kemna and N. Zisser, 2007. Hydraulic conductivity estimation from induced polarisation data at the field scale—the Krauthausen case history. Journal of Applied Geophysics, 62: 33-46.

Hördt, H., A. Druiventak, R. Blaschek, F. Binot, A. Kemna, P. Kreye and N. Zisser, 2009. Case histories of hydraulic conductivity estimation with induced polarization at the field scale. Near Surface Geophysics, 7: 529-545.

Jordan, H., 1975. Erlaeuterungen zu Blatt Grossburgwedel Nr. 3525. Niedersaechsisches Landesamt fuer Bodenforschung, Hannover, 93.

Kemna, A., 2000. Tomographic inversion of complex resistivity theory and application. Ph.D. thesis, Bochum Univ., Germany.

Kemna, A., A. Binley, G. Cassiani, E. Niederleithinger, A. Revil, L. Slater, K. Williams, A. Flores Orozco, F-H. Haegel, A. Hördt, S. Kruschwitz, V. Leroux, K. Titov and E. Zimmermann, 2012. An overview of spectral induced polarization method for near-surface applications. Near Surface Geophysics, 10,xxx-xxx, doi:10.3997/1873-0604.2012027.

Kemna, A., A. Binley and L. Slater, 2004. Crosshole IP imaging for engineering and environmental applications. Geophysics, 69: 97-107.

Kilner, M., L. West and T. Murray, 2005. Characterization of glacial sediments using geophysical methods for groundwater source protection. Journal of Applied Geophysics, 57: 293-305.

Klein, J.D. and W.R. Sill, 1982. Electrical properties of artificial clay-bearing sandstone. Geophysics, 47: 1593-1605.

Klitzsch, N., 2004. Ableitung von Gesteinseigenschaften aus Messung der Spektralen Induzierten Polarisation (SIP) an Sedimentgesteinen. Ph.D. thesis, TU Univ., Leipzig, Germany.

Lange, G. and F. Jacobs, 2005. Electromagnetic methods. In: Environmental Geology: handbook of field methods and case studies, Eds., Knoedel. K., G. Lange. Springer Verlag, Berlin, pp: 239-282.

Loke, M.H. and R.D. Barker, 1996. Rapid least-squares inversion of apparent resistivity pseudo-sections using quasi-Newton method. Geophysical Prospecting, 44: 131-152.

Radic, T., 2004. Elimination of cable effects with multichannel SIP measurements. Ext. Abstr., 10th Eur. Mtg. Env. Eng. Geophysics, Utrecht.

Radic, T., D. Kretzschmar and E. Niederleithinger, 1998. Improved characterization of unconsolidated sediments under field conditions based on complex resistivity measurements. Ext. Abstr., 4th Eur. Mtg. Env. Eng. Geophysics, Barcelona.

Revil, A. and N. Florsch, 2010. Determination of permeability from spectral induced polarization in granular media. Geophysical Journal International, 181(3): 1480-1498.

Seidel, K. and G. Lange, 2005. Direct resistivity methods. In: Environmental Geology: handbook of field methods and case studies, Eds., Knoedel, K., G. Lange and H.-J. Voigt. Springer Verlag, Berlin, pp: 205-237.

Slater, L. and D. Lesmes, 2002. IP interpretation in environmental investigations. Geophysics, 67: 77-88.

Sturrock, J.T., D. Lesmes and F.D. Morgan, 1998. The influence of micro-geometry on the hydraulic permeability and induced polarization response of sandstones. In the proceedings of the symposium on the application of geophysics to engineering and environmental problems, pp: 859-867.

Vanhala, H., 1997. Laboratory and field results of the use of spectral induced-polarization (SIP) method for detecting organic and inorganic contaminants. In the proceedings of the 3rd EEGS-ES meeting, Aarhus, DK, pp: 37-40.

Weller, A., L. Slater, S. Nordsiek and D. Ntarlagiannis, 2010. On the estimation of specific surface per unit pore volume from induced polarization: A robust empirical relation fits multiple datasets. Geophysics, 75(4): WA105-WA112.

Xiang, J.N.B., D. Jones, D. Cheng and F.S. Schlindwein, 2002. A new method to discriminate between a valid IP response and EM coupling effects. Geophysical Prospecting, 50: 566-576.

Zanetti, C., A. Weller, M. Vennetier and P. Mériaux, 2011. Detection of buried tree root samples by using geoelectrical, measurements: a laboratory experiment. Plant and Soil, 339: 273-283.